Intelligent Control of Pulsed GTAW with Filler Metal

The dynamic neural network model accurately predicted backside width and topside height and could be used for process control

BY G. J. ZHANG, S. B. CHEN, AND L. WU

ABSTRACT. This paper addresses intelligent control of weld shape for plates with varied root openings during pulsed GTAW with filler metal, and is a development from the work in Refs. 1–3. The newly developed double-sided visual image sensing system could acquire the front topside, back topside, and backside images of the weld pool simultaneously in the same frame. The root opening and the double-sided weld pool geometry parameters were extracted online. A neural network model was established to predict the backside width and topside height through welding parameters and topside shape parameters. Feasible intelligent control schemes were also investigated. In order to eliminate the effect of the root opening and stabilize both backside width and topside height, a double-variable controller was designed, in which the feedback control part regulates the pulse duty ratio to control backside width and, at the same time, the feed-forward control part adjusts the filler metal rate to achieve the desired topside height in order to compensate for the effects of the varying root openings.

Introduction

This paper studies weld shape quality control in pulsed gas tungsten arc welding (GTAW-P) with a filler metal, and is a development from the work in Refs. 1–3. The state of the art of weld shape quality control has been reviewed in detail in those papers. By summarizing Refs. 1–32, the following can be seen:

1. Although extensive research has been done to find feasible approaches for the adaptive control of the complicated welding process, more practical solutions are still strongly needed for different cases (Refs. 4–8).

2. Among the studied sensing methods, passive visual image sensing has proven to be a feasible and promising method (Refs. 9–25).

3. With regard to modeling and controlling the welding process, artificial intelligence methodology was thought to be a feasible tool for the complex nonlinear system (Refs. 26–28), and some studies have been done that showed promising results (Refs. 29–32).

4. Most research has centered on bead-on-plate and GTA welding of butt joints without a root opening and filler metal; welding with filler metal and a root opening has not been addressed adequately.

Unfortunately, in practical welding, variation in root opening is unavoidable and affects the resultant weld shape and quality. Especially when the root opening is too large, incision will occur and joining is not obtained.

Research on intelligent control of weld pool shape during pulsed GTAW at Harbin Institute of Technology has gone through three stages: bead-on-plate (Ref. 2), welding of butt joints without filler metal (Ref. 3), and welding of butt joints with filler metal (Ref. 1). The results of this research were published in a series of papers in the *Welding Journal* (Refs. 1–3). As a continuation, this paper took into account the existence of the root opening and its effect on weld shape, and established an intelligent control system for weld shape quality during pulsed GTAW of butt joints with varied root openings.

In this paper, first, a new double-sided imaging system for the weld zone was developed to acquire the front topside, back topside, and backside images of the weld pool simultaneously in the same frame. Second, a neural network model of the dynamic process was established to predict backside width and topside height through welding parameters and topside shape parameters. Finally, a double-variable composite intelligent controller was developed and studied.

KEYWORDS

Vision Sensing
Neural Network
Intelligent Control
Root Opening
Weld Geometry Shape
Pulsed GTAW
Filler Metal
Fuzzy Control
Double-variable Composite Control

G. J. ZHANG and L. WU are with National Key Laboratory of Advanced Welding Production Technology, Harbin Institute of Technology, Harbin, P.R.China. S. B. CHEN is with Institute of Welding Technology, Shanghai Jiao Tong University, Shanghai, P.R. China.

Sensing

System

The experimental system was the same as the one in Ref. 1; however, certain modifications were made.

First, an isolated gate bipolar transistor (IGBT) switch power source was used as the welding machine whose dynamic response time was less than 1 ms.

Second, in order to clearly view the root opening from the front of the weld pool, the wire was filled at 15 deg, deviating from the weld joint from the front. The wire was fed during the peak current period. The filling time was fixed at 300 ms; the filling amount was adjusted by regulating the feeding rate.

In order to sense the shape of the weld pool and the joint root opening, a new imaging light path was developed to acquire the front topside, back topside, and backside images of the weld pool simultaneously in the same frame.

This new light path system is shown in Fig. 1, and has been designed to guarantee the three weld pool images to be clearly and simultaneously formed on the same CCD camera.

In Fig. 1, O_XYZ is the workplate coordinate system. Point O is the center point of the weld pool image. The positive direction of axis X is the welding direction. The front topside imaging light path is composed of the reflecting mirrors M_1 and M_2, the back topside imaging light path consists of the reflecting mirrors M_3 and M_4, and the backside imaging light path is formed by the reflecting mirrors M_5, M_6, and M_7.

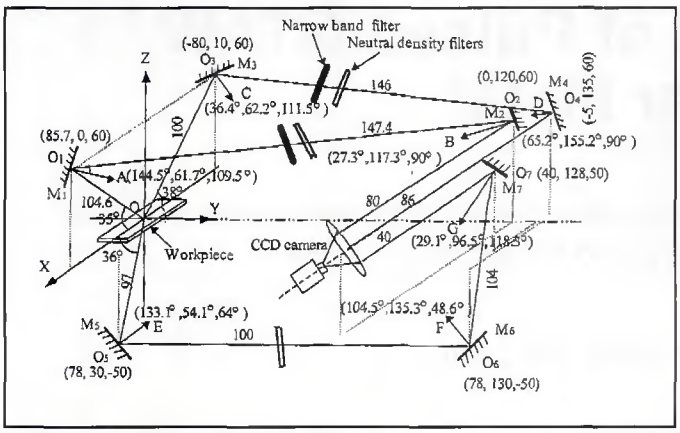

Fig. 1 — Schematic diagram of the light path.

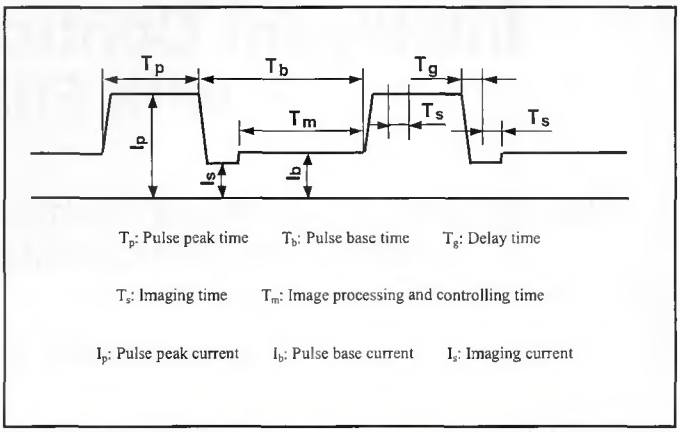

Fig. 2 — Current waveform.

Table 1 — Experimental Condition for Image Sensing

Pulse frequency f (Hz)	Peak current I_p (A)	Base current I_b (A)	Welding speed V_w (mm/s)	Filler rate V_f (cm/s)	Arc length l (mm)	Electrode diameter Φ (mm)	Angle of tip θ (deg)	Ar Flow rate l (l/min)	Pulse Duty ratio (%)
1	130	40	2.5	5	3.0	3.0	30	8.0	50

Weld Pool Images

Experiments with groove welds in a butt joint with a root opening were done on low-carbon steel Q235B. The experiment conditions are tabulated in Table 1.

The waveform of the current is shown in Fig. 2. The images were separately acquired during the peak and base current periods to study for the optimal imaging time and imaging current.

Figure 3 shows the double side pool images sensed under the above experimental conditions. Each image consists of three sub-images acquired from the three different directions as illustrated in Fig. 3F.

Experimental observation and study suggests the following optimal imaging time: the front topside pool image be sampled 60 ms before the end of the pulse peak current to extract the root opening; the back topside image and backside image be acquired 100 ms after the start of the base current to obtain the feedback for intelligent control of the backside width and topside height.

As shown in Ref. 1, the topside length L_t, maximum width W_t, and half-length ratio R_{hl} and topside height H_t can be used as the characteristic parameters to describe the shape and size of the topside weld pool. The backside pool is specified by the maximum width W_b and length L_b.

A real-time image processing algorithm has been developed to extract the root opening, and the topside and backside weld pool shape parameters.

Neural Network Modeling

The backside width and the topside height are the key variables that determine the weld shape. Unfortunately, the topside height could not be directly extracted and the backside width could not be directly sensed either in most cases. So, a dynamic process model should be established to predict the backside width and the topside height by the topside pool geometry parameters and the welding parameters. Neural network modeling is an appropriate modeling method for the complex process.

Model Structure

Figure 4 shows the architecture of the model for predicting the backside width and topside height (BWHDNNM). The model inputs were the welding parameters (peak current I_p, pulse duty ratio δ, welding speed V_w, filler rate V_f), root opening g, topside pool shape parameters (L_t, W_t, and R_{hl}), and their history values at two former pulses, a total of 24 numbers. The model outputs were the current backside width and topside height. The number of elements in the hidden layer was set at 10 by a trial and error procedure. S function was chosen as the transfer function of the neural element.

Experiment for the Training Data

Experiments were carried out on 2-mm-thick low-carbon steel plates for pulsed GTAW of butt joints with a root opening. The basic experiment conditions are shown in Table 1. To excite all the characteristics of the dynamic welding process, the inputs were designed with white noise signals because of their characteristics of widespread spectrum and noncorrelation on time. Through experiments, the following welding parameters were chosen as the operating point under which the satisfactory weld bead geometry could be obtained, Ip_0 = 135 A, δ_0 = 50%, V_{w0} = 2.5 mm/s, V_{f0} = 5 cm/s. The range of the inputs were set as follows: $\Delta Ip = \pm 20$ A, $\Delta\delta = \pm 10\%$, $\Delta V_w = \pm 0.5$ mm/s, $\Delta V_f = \pm 4$ cm/s. The corresponding varying steps were 5 A, 5%, 0.17 mm/s, and 1 cm/s. In welding with a root opening, a 1-mm root opening was preset when the workplate was clamped. Due to heat distortion of the plate, the root opening varied during welding, as seen in Fig. 5A.

The number of the welding pulse current on every work plate was 90, and 30 groups of experiments were conducted, 10 groups of which were on workplates without a root opening, the other 20 groups were with a root opening. The root opening g and the weld pool two-dimensional plate geometry parameters (W_t, L_t, R_{hl}, W_b) were sensed online by the previously mentioned developed imaging system and image processing algorithm. The experiment results are shown in Fig. 5. The topside height H_t was measured off-line. In pulsed welding, there are ripples on the

surface of the weld, so the weld pool boundary of every pulse can be easily identified. When measured, the welded workpiece was fixed on the movable platform of the structured light height measurement system.

Twenty-five hundred sample data pairs were obtained.

Training and Testing

The training of the previously mentioned neural networks was performed using a self-developed algorithm that used the Levenberg-Marquardt rule as the learning algorithm. The first 2200 of the entire 2500 sample data were taken as training data, the following 100 were used as validation data, and the last 200 data were used as testing data.

Test results of the BWHDNNM model are shown in Fig. 6. Error statistical data showed the mean errors of the backside width and topside height between the predicted and the measured were –0.0146 and 0.0613 mm, respectively, and the relative mean square errors were 4.63 and 6.7%, respectively. The testing results verified the feasibility of the developed models.

Intelligent Control for the Weld Shape

Two intelligent control systems, the single variable and double variable, were developed.

Single-Varlable Self-learning Fuzzy Neural Network Control

During the design of the general fuzzy logic controller, the difficulty was the decision of the membership functions and the fuzzy rules. Fortunately, the fuzzy system can be expressed by an equivalence neural network; the neural network is no longer a black box, its every layer and every node are related to a part of the fuzzy system, and all nodes and weights have certain physical meanings that correspond to the membership functions and inference process. So, the membership functions and inference rules can be decided through the learning of the neural network, which makes the fuzzy controller have the ability of self-learning and self-adaptation.

The structure of the fuzzy neural network, fuzzy inference process, and learning algorithm can be seen in Ref. 3.

Control System

The fuzzy neural network controller (FNNC) for the backside width is shown in Fig. 7. MS was the measuring system for detecting the topside shape parameters TSP (L_t, W_t, and R_{hl}) and the welding parameters WP, such as welding current, travel speed, etc. These detected parameters were input into the ANN predicting model BWHDNNM, and the predicted backside width W_{bp} was generated by BWHDNNM. The error e between the given backside width W_{bset} and the feedback backside width W_{bp} was input into the FNNC. The FNNC regulated the controlling variable, namely the pulse duty ratio δ, to keep the backside width stable.

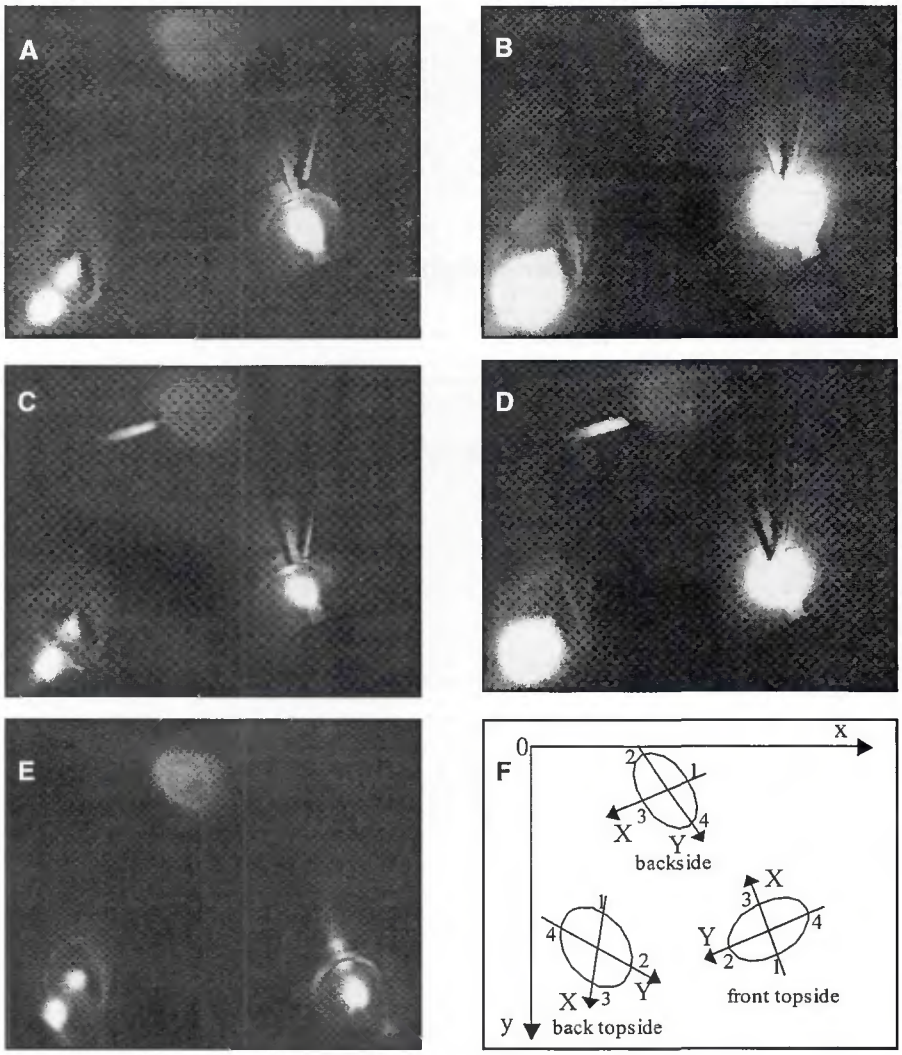

Fig. 3 — Weld pool images. A — Butt joint with no root opening at base current period; B — butt joint with no root opening at peak current period; C — butt joint with large root opening at base current period; D — butt joint with large root opening at peak current period; E — bead-on-plate weld at base current period; and F — schematic diagram of the calibrations.

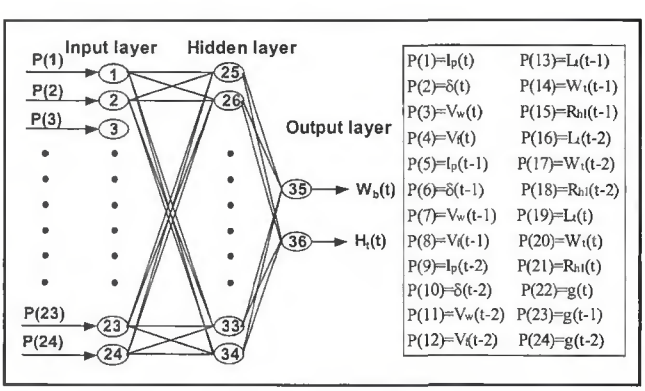

Fig. 4 — Structure for predicting the backside width and topside height.

Simulation

Simulations of the FNNC performance were conducted in four cases. W_{bset} is the

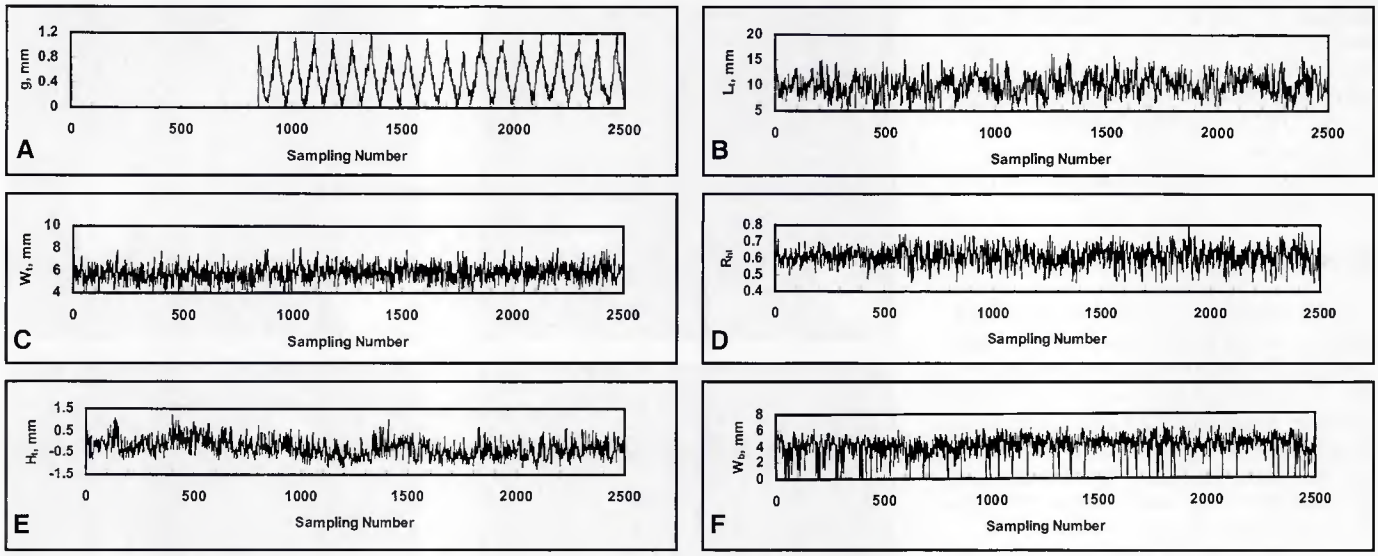

Fig. 5 — The measured shape parameters of the weld pool. A — Root opening; B — L_t; C — W_t; D — R_{hl}; E — H_t; F — W_b.

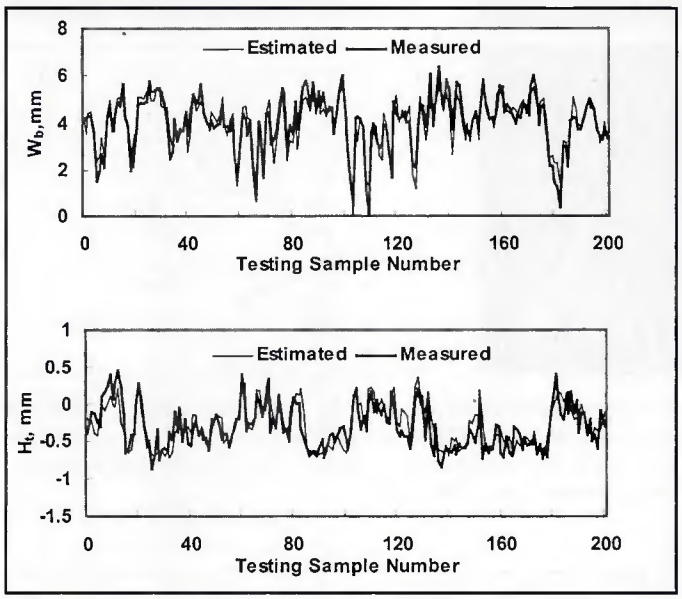

Fig. 6 — Test results of BWHDNNM.

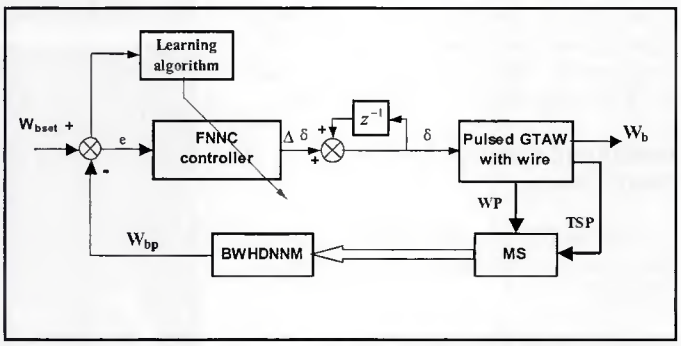

Fig. 7 — Schematic diagram of FNNC closed-loop control system.

following in the four cases: 3.5 mm without root opening, 5.0 mm without root opening, 5.0 mm with 0.4-mm root opening, and 5.0 mm with 0.6-mm root opening. The minimum regulating unit was 1% for pulse duty ratio. The symbol *e* denotes the error of the backside width W_b (its range is –2.0 to 2.0 mm); *ce* denotes the error change (its range is –1.5 to 1.5 mm); *cu* denotes the variety of the pulse duty ratio (its range is –15% to 15%). The initial welding conditions were I_p = 130 A, δ = 40%, V_w = 2.5 mm/s, and V_f = 5.0 cm/s. The simulation results were shown in Fig. 8. It could be seen that the FNNC had small overshoot, quick adjusting speed, and could adapt the varying of the controlled object characteristics.

Control Experiment

To verify the performance of the FNNC, experiments on butt joint welds with filler metal were conducted on varied heat-sink workplates and varied root opening workplates. The size of the varied root opening pieces is shown in Fig. 9. The controlled variable of the backside width was set as 5 mm. The minimum regulating unit of pulse duty ratio was 1%. The control functioned from pulse 7.

In order to avoid the clamping condition's effect on the results, the clamping plates were used instead of the clamping block. Each of the clamping plates has the same length as the workplates. The two ends of the workplate were joined by spot weld.

The control results are shown in Figs. 10–12. Figure 10 shows the variation in shape parameters. Figure 11 shows the double-sided pool images. The photographs in Fig. 12 show the surfaces of the resultant weld.

Statistic results show the maximum error between the real value and the given value was 0.39 mm, the mean error was 0.014 mm, and the root mean square was 0.14 mm. The real backside width was maintained around the given value of 5 mm, but the topside surface sank at the root opening.

Double-Variable Composite Controller

The FNNC experiment described in the previous section, in which root opening was considered as a disturbance, showed that root opening was a very important factor to weld shaping. Regulating pulse duty ratio only could keep backside width stable, but the topside surface sank at the root opening. In addition, a large root opening can easily induce cutting. So the right operation was to regulate the filler rate online by the size of the root opening, which could achieve the desired positive reinforcement.

Parameter Preset Feed-Forward Control

In this experiment system, root opening can be measured online, so it is possible to preset the filler rate by the size of the root opening. The key question was to decide what rate should be preset.

Choose a working point (I_p = 130 A, t_p = 50%, V_w = 2.5 mm/s, V_f = 5 cm/s) at which the topside height was zero in the case of welding with no root opening. Then, the welding with varied root openings was done. At the root opening, the filler rate was stepped up until the topside height became zero. The increment of the filler rate was regarded as compensation value.

In order to reduce the experiment workload, the simulation experiment was carried out to get the initial compensation value at different root openings. Figure 13 shows the topside height control principle used in the simulation experiment.

The compensation value obtained from the simulation was revised by a real welding experiment. Table 2 shows the compensation value finally decided upon for the filler rate at different root openings.

Table 2 — The Compensating Value of Filler Rate for Different Root Openings

Root opening (mm)	0.1	0.2	0.3	0.4	0.5	0.6	0.7	0.8	0.9	1
ΔV_f (cm/s)	0.2	0.4	0.7	1	1.5	2	2.4	2.8	3.1	3.5
V_f (cm/s)		≥ 2	≥ 3	≥ 4	≥ 4	≥ 5	≥ 6	≥ 6	≥ 7	≥ 7

The preset filler rate had a minimum in order to avoid cutting at different root openings, which is shown in the third row of Table 2.

Double-Variable Composite Control

As known from the previously described control experiment, in the case of varied root openings, the single-variable feedback controller could keep the backside width stable by regulating the pulse duty ratio, but the topside height was not constant. Especially at a large root opening, the topside surface sank severely. On the other hand, the feed-forward control strategy of presetting the filler rate according to size of the root opening could eliminate the effect of the root opening on the topside height, but could not guarantee backside width uniformity. So a double-variable composite controller should be designed in order to stabilize both backside width and topside height by simultaneously regulating pulse duty ratio and filler rate. In the designed composite controller, the feedback control part regulated pulse duty ratio to stabilize the backside width, while at the same time, the feed-forward control part adjusted the filler rate to eliminate topside caving due to root opening. The control principle is shown in Fig. 14.

In order to validate the designed dou-

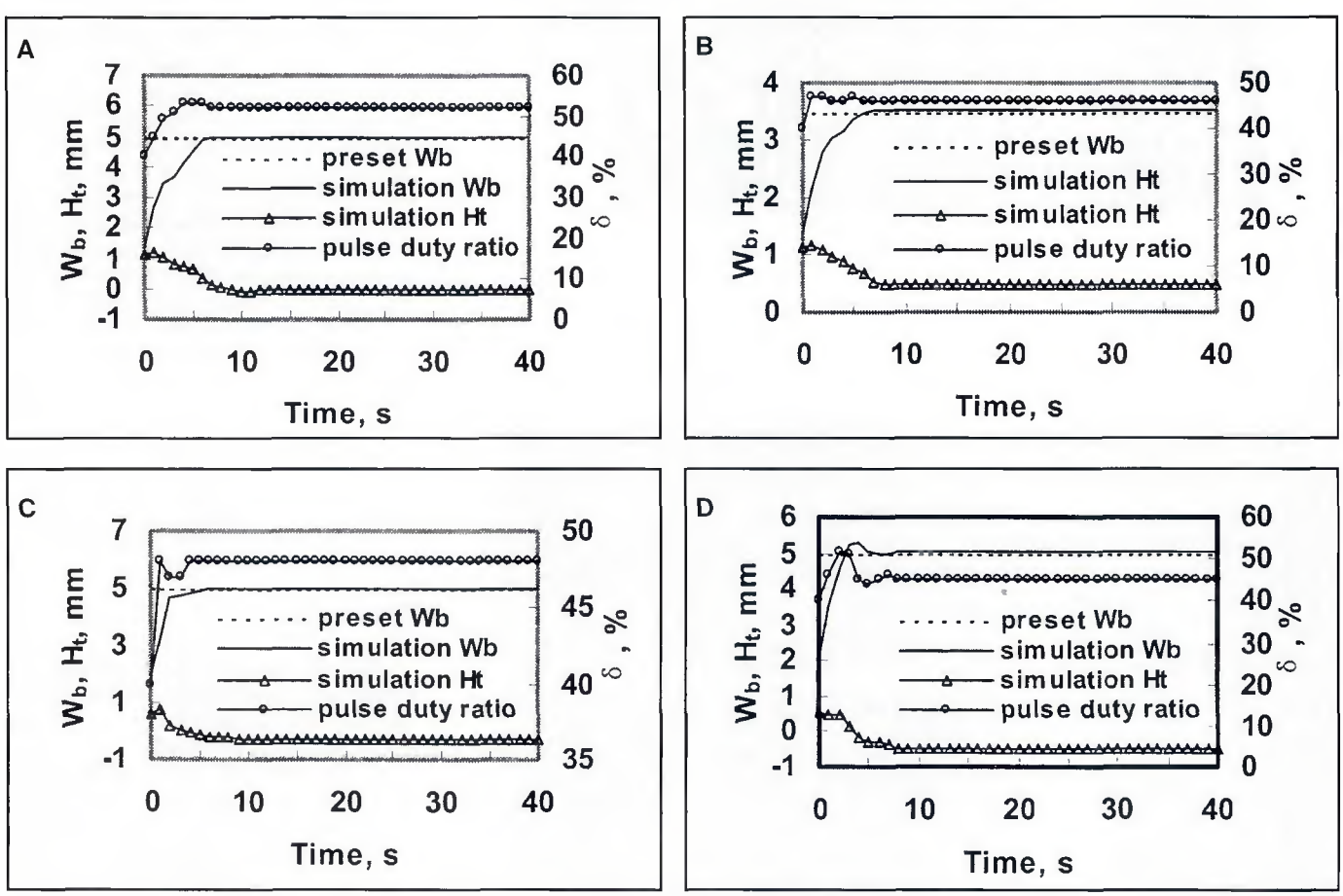

Fig. 8 — Simulation of FNNC. A — Root opening = 0, W_b = 5.0 mm; B — root opening = 0, W_b = 3.5 mm; C — root opening = 0.4 mm, W_b = 5.0 mm; D — root opening = 0.6 mm, W_b = 5.0 mm.

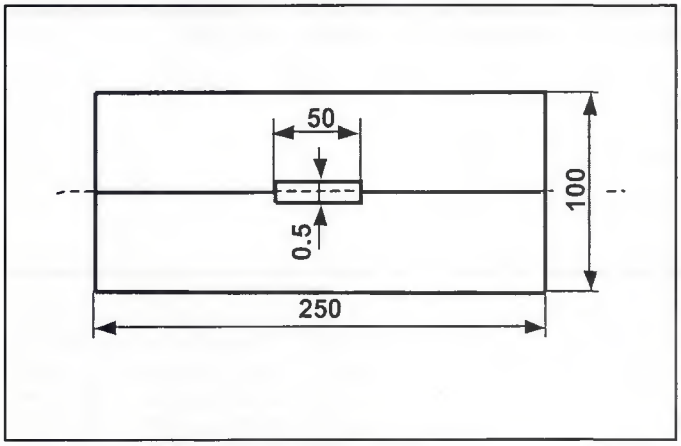

Fig. 9 — Workplate with varied root opening.

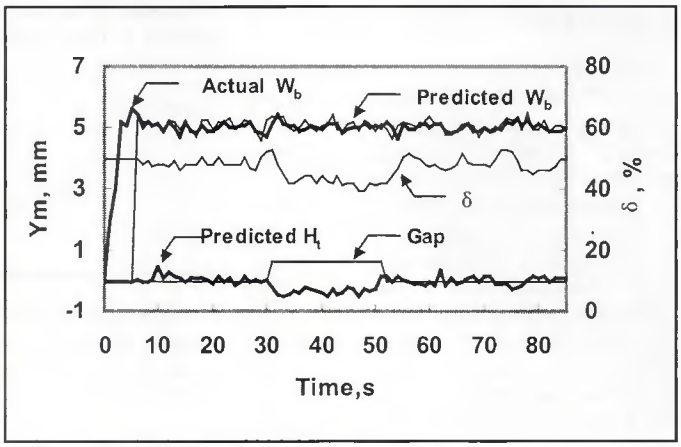

Fig. 10 — FNNC closed-loop experimental results on plate with varied root openings.

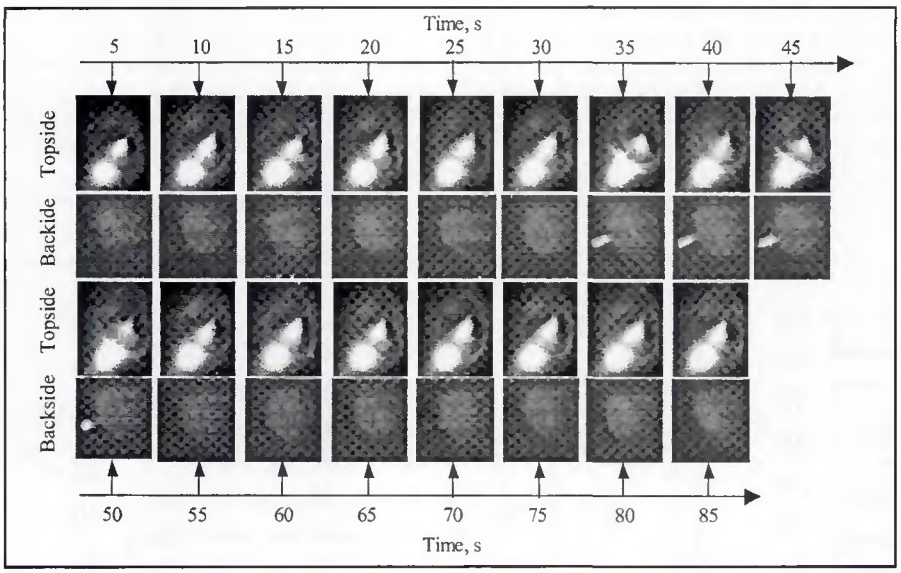

Fig. 11 — Weld pool images in single-variable FNNC experiment.

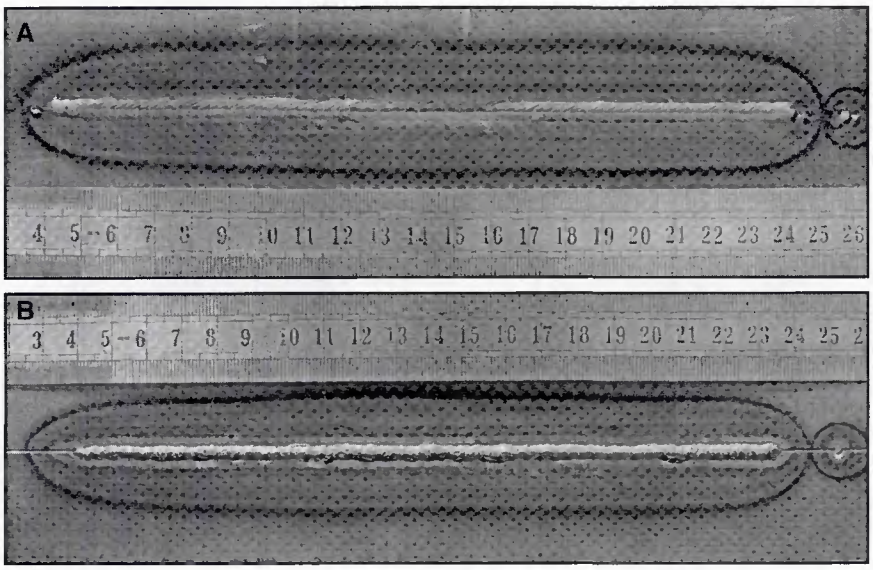

Fig. 12 — Weld made in FNNC closed-loop experiment. A — Topside; B — backside.

ble-variable composite controller, a real control experiment was done at the varied root opening workplate shown in Fig. 15. The desired output of the backside width was set at 5 mm. Figure 16 shows the regulating curve of the control process. The welded workplate is shown in Fig. 17.

Experiment results showed the real backside weld width W_b maintained at 5.0 mm. By statistic, the maximum error between W_b and W_{bset} was 0.32 mm, the average error was 0.02 mm, and the root-mean-square error was 0.18 mm. The average topside height was –0.018 mm, the root-mean-square error was 0.08 mm, and the maximum error was 0.09 mm. As seen from the control results, in the case of varied root openings, the double-variable composite controller not only could guarantee the backside width uniformity, but also could guarantee the topside height had no significant difference when the root opening varied. The control results of the double-variable composite controller could satisfy the requirement for weld shaping at most applications. It was seen from the control process that the pulse duty ratio was regulated at a smaller range, compared to Fig. 10, due to the compensation of the preset filler metal rate to the root opening.

Conclusions

With the existence of root opening, the intelligent techniques for weld shape control were investigated and the following conclusions were obtained.

1. The newly developed multiorientation visual sensing system has realized simultaneous image sensing of front topside, back topside, and backside weld pool in a frame during pulsed GTAW with filler metal. The sampled images had acceptable resolution and contrast, and provided information about the dynamic weld pool.

2. The constructed dynamic neural net-

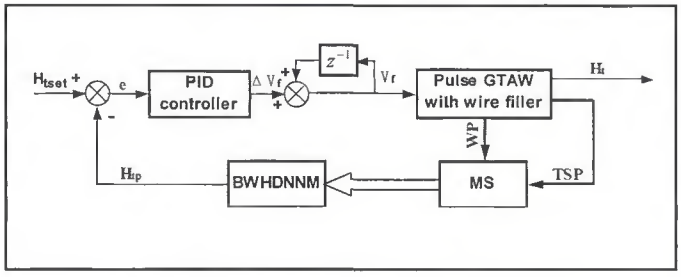

Fig. 13 — Schematic diagram of simulation.

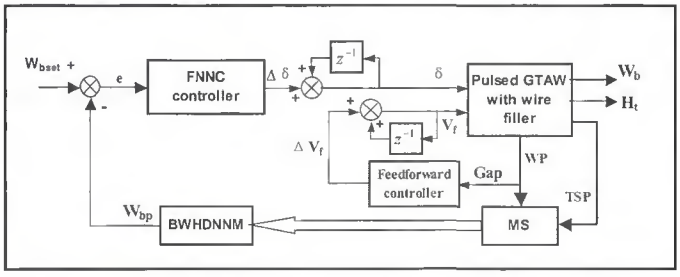

Fig. 14 — Schematic diagram of the double-variable complex controller.

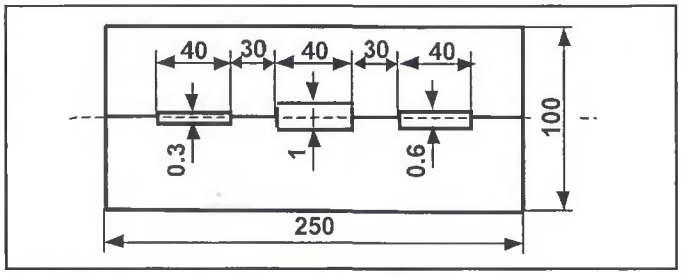

Fig. 15 — Sketch of workplate with varied root openings.

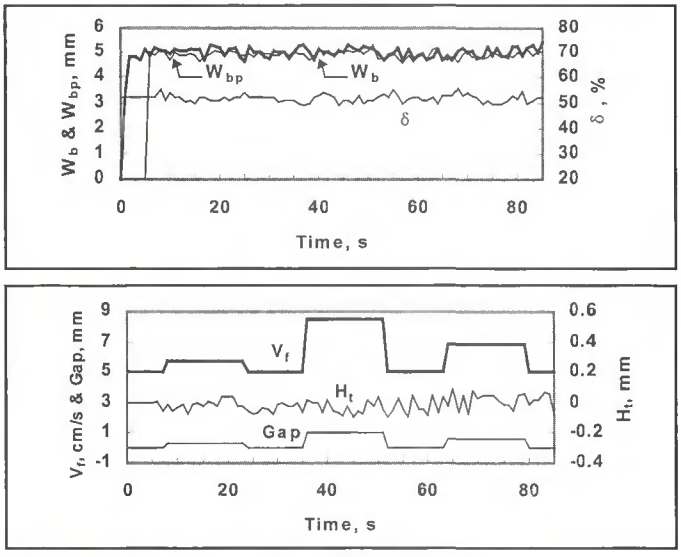

Fig. 16 — Double-variable complex control experiment.

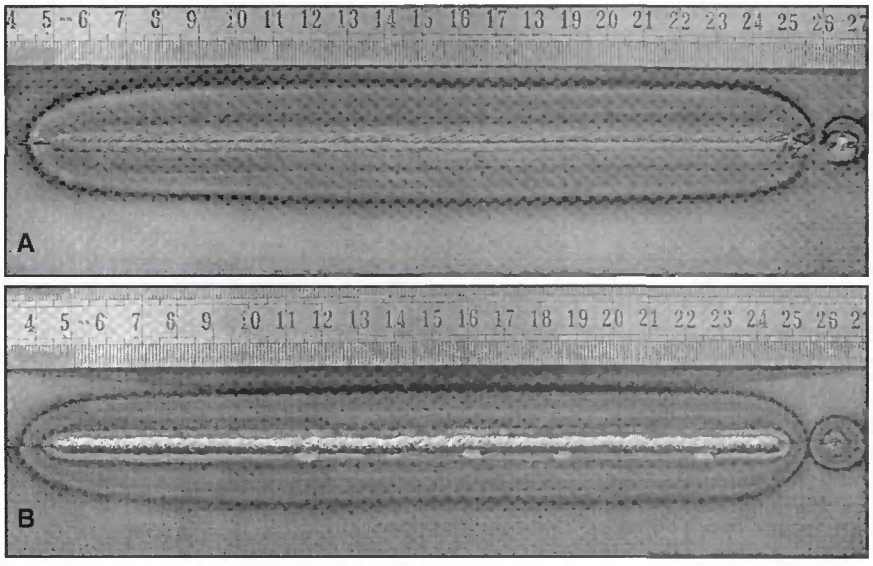

Fig. 17 — Weld made in the double-variable complex control experiment. A — Topside; B — backside.

work model could accurately predict the backside width and topside height through welding parameters and topside shape parameters. The validating experiment results proved that the model had high accuracy and could be used in process control.

3. The experiment results of the developed SISO self-learning fuzzy neural network controller showed the following:

- For the welding process with time-varying conditions, the intelligent controller with the function of online self-learning had adequate adaptive capability, and could achieve satisfactory control performance under different conditions.
- For welding with varied root openings, the backside width was easily kept stable. However, the topside height was not controlled; when the root opening was large, the topside surface sank severely. Hence, for large root openings, a double-variable controller should be considered.

4. The designed double-variable composite controller can stabilize both backside width and topside height by simultaneously adjusting pulse duty ratio and filler rate.

Acknowledgment

This work was supported by the National Natural Science Foundation of China (No. 59635160) and Visiting Scholar Foundation of Key Laboratory in China University.

References

1. Zhao, D. B., Chen, S. B., Wu, L., Dai, M., and Chen, Q. 2001. Intelligent control for the shape of the weld pool in pulsed GTAW with filler metal. *Welding Journal* 80(11): 253-s to 260-s.

2. Chen, S. B., Lou, Y. J., Wu, L., and Zhao, D. B. 2000. Intelligent methodology for sensing, modeling and control of pulsed GTAW: Part 1 — Bead-on-plate welding. *Welding Journal* 79(6): 151-s to 163-s.

3. Chen, S. B., Zhao, D. B., Wu, L., and Lou, Y. J. 2000. Intelligent methodology for sensing, modeling and control of pulsed GTAW: Part 2 — Butt joint welding. *Welding Journal* 79(6): 164-s to 174-s.

4. Wikle III, H. C., Kottilingam, S., Zee, R.

H., and Chin, B. A. 2001. Infrared sensing techniques for penetration depth control of the submerged arc welding process. *Journal of Materials Processing Technology* 113(6): 228–233.

5. Ward, P. 2001. Improving productivity with robotic welding. *Welding Journal* 80(8): 52–54.

6. Kannatey-Asibu, E. 1997. Milestone developments in welding and joining processes. *ASME Journal of Manufacturing Science and Engineering* 119(11): 801–810.

7. Nagesh, D. S., and Datta, G. L. 2002. Prediction of weld bead geometry and penetration in shielded metal arc welding using artificial neural networks. *Journal of Materials Processing Technology* 123(2): 303–312.

8. Li Di, Srikanthan, T., Chandel, R. S., and Katsunori. 2001. Neural-network-based self-organized fuzzy logic control for arc welding. *Engineering Applications of Artificial Intelligence* 14(2): 115–124.

9. Bentley, A. E., and Marburger, S. J. 1992. Arc welding penetration control using quantitative feedback theory. *Welding Journal* 71(11): 397-s to 405-s.

10. Duley, W. W., and Mao, Y. L. 1994. Effect of surface condition on acoustic emission during welding of aluminum with CO_2 laser radiation. *Journal of Physics D: Applied Physics* 27(7): 1379–1383.

11. Renwick, R. J., and Richardson, R. W. 1983. Experimental investigation of GTA weld pool oscillations. *Welding Journal* 62(2): 29-s to 35-s.

12. Zacksenhouse, M., and Hardt, D. E. 1983. Weld pool impedance identification for size measurement and control. *ASME Journal of Dynamics Systems, Measurement, and Control* 105(3): 179–184.

13. Xiao, Y. H., and Ouden, G. den. 1993. Weld pool oscillation during GTA welding of mild steel. *Welding Journal* 72(8): 428-s to 434-s.

14. Yoo, C. D., and Richardson, R. W. 1993. Experimental study on sensitivity and signal characteristics of weld pool oscillation. *Transactions of the Japan Welding Society* 24(2): 54–62.

15. Hardt, D. E., and Katz, J. W. 1984. Ultrasonic measurement of weld penetration. *Welding Journal* 63(9): 273-s to 281-s.

16. Nagarajan, S., Chen, W. H., and Chin, B. A. 1989. Infrared sensing for adaptive arc welding. *Welding Journal* 68(11): 462-s to 466-s.

17. Chen, W., and Chin, B. A. 1990. Monitoring joint penetration using infrared sensing techniques. *Welding Journal* 69(4): 181-s to 185-s.

18. Richardson, R. W., Gutow, D. A., Anderson, R. A., and Farson, D. F. 1984. Coaxial arc weld pool viewing for process monitoring and control. *Welding Journal* 63(3): 43–50.

19. Kovacevic, R., Zhang, Y. M., and Li, L. 1996. Monitoring of weld joint penetration based on weld pool geometrical appearance. *Welding Journal* 75(10): 317-s to 329-s.

20. Agapakis, J. E., and Bolstad, J. 1991. Vision sensing and processing system for monitoring and control of welding and other high luminosity processes. *International Robots & Vision Automation Conference*, pp. 23–28.

21. Zhang, Y. M., Li, L., and Kovacevic, R. 1995. Monitoring of weld pool appearance for penetration control. *4th International Conference on Trends in Welding Research*, Gatlinburg, Tenn., pp. 30–35.

22. Oshima, K., and Morita, M. 1992. Sensing and digital control of weld pool in pulsed MIG welding. *Transactions of the Japan Welding Society* 23(4): 36–42.

23. Kim, E. W., Allemand, C., and Eagar, T. W. 1987. Visible light emissions during gas tungsten arc welding and its application to weld image improvement. *Welding Journal* 66(12): 369-s to 377-s.

24. Brzakovic, D., and Khani, D. T. 1991. Weld pool edge detection for automated control of welding. *IEEE Transactions on Robotics and Automation* 7(3): 397–403.

25. Pietrzak, K. A., and Packer, S. M. 1994. Vision-based weld pool width control. *ASME Journal of Engineering for Industry* 116: 86–92.

26. Andersen, K., and Cook, G. E. 1990. Artificial neural networks applied to arc welding process modeling and control. *IEEE transaction Industry Application* 26(9): 824–830.

27. Yasuo SUGA, Takahiro, S., Shigeaki, U., and Kimiya, A. 1999. Measurement of molten pool shape and penetration control applying neural network in TIG welding of thin steel plates. *ISIJ International* 39(10): 1075–1080.

28. Cook, G. E., Barnett, R. J., Andersen, K., and Strauss, A. M. 1995. Weld modeling and control using artificial neural networks. *IEEE Transactions on Industry Applications* 31(6): 1484–1491.

29. Lim, T. G., and Cho, H. S. 1993. Estimation of weld pool sizes in GMA welding process using neural networks. *Journal of Systems and Control Engineering* 207(1): 15–26.

30. Andersen, K., Cook, G. E., and Barnett, R. J. 1992. Gas tungsten arc welding process control using artificial neural networks. *Proceedings of the 3rd International Conference on Trends in Welding Research*, Gatlinburg, Tenn., pp. 877–881.

31. Kovacevic, R., and Zhang, Y. M. 1997. Neurofuzzy model-based weld fusion state estimation. *IEEE Control Systems Magazine* 17(2): 30–42.

32. Chen, S. B., Wu, L., and Wang, Q. L. 1997. Self-learning fuzzy neural networks for control of uncertain systems with time delay. *IEEE Transactions on System, Man, and Cybernetics-Part B: Cybernetics* 27(2): 142–148.